Analytical Methods

Accepted Manuscript

This article can be cited before page numbers have been issued, to do this please use: W. Li, J. Li, S. Sun, M. Duan, M. Wang and R. Wang, *Anal. Methods*, 2025, DOI: 10.1039/D5AY01118C.

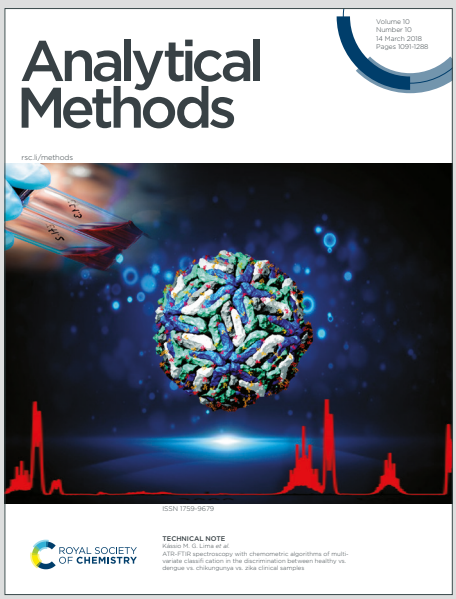

ROYAL SOCIETY OF CHEMISTRY

rsc.li/methods

View Article Online
DOI: 10.1039/D5AY01118C

ARTICLE

Isothermal amplification-bridged ratiometric DNA switch for sensitive detection of viral gene fragments

Wei Li,*[a] Jiayue Li,[b] Shang Sun,[a] Manman Duan,[a] Meng Wang,[b] and Rui Wang*[a]

Received 00th January 20xx,
Accepted 00th January 20xx

DOI: 10.1039/x0xx00000x

The detection of viral gene fragments is essential for diagnosing and screening viral infections, managing virus transmission, and controlling epidemics. In this study, we developed an isothermal amplification-bridged DNA switch designed for the sensitive detection of viral gene fragments. Specifically, the binding of the target viral gene fragment to the recognition sequences triggers isothermal amplification, resulting in the production of multiple DNA products. Consequently, a single target gene fragment is transformed into approximately 1,250 DNA products, which can subsequently activate the DNA switches. This activation leads to the opening of the DNA switch and the occurrence of Förster resonance energy transfer (FRET), generating a ratiometric fluorescent signal. The effective conversion of the target facilitated by isothermal amplification enables the generation of amplified ratiometric fluorescent signals, thereby achieving sensitive detection of the severe acute respiratory syndrome coronavirus 2 (SARS-CoV-2) gene fragment with a limit of detection of 0.04 fM. An extensive linear range spanning approximately eight orders of magnitude, characterized by two distinct linear relationships, is obtained, making it particularly effective for detecting viral gene fragments in various biological samples with significantly varying concentrations of target gene fragments. The analysis of actual samples from patients presenting with upper respiratory symptoms underscores the method's potential for clinical diagnostic applications. Additionally, by modifying the recognition strands, the method allows for the sensitive and selective detection of the Rabies virus (RABV) gene fragment, highlighting its versatility and adaptability. Therefore, this research presents a novel and sensitive approach for detecting of viral gene fragments, offering considerable promise for the clinical diagnosis of infectious diseases.

1. Introduction

The prompt and precise diagnosis of viral infections is crucial for managing the transmission of viruses and assessing disease progression.[1] Diagnostic approaches for viral infections include serological tests and nucleic acid assays.[2] Typically, serological test targets viral antigens or their corresponding antibodies. However, these tests can be significantly affected by the status and concentration of antigens, potentially resulting in ambiguous diagnostic outcomes.[2,3] Additionally, the generation of detectable antibodies in patients may take several days to weeks, which can further delay the identification of viral infections.[4] In contrast, nucleic acid assay focus on specific viral gene fragments and provides a highly sensitive and precise approach for diagnosing viral infections, with polymerase chain reaction (PCR) recognized as the gold standard technique.[5] Nonetheless, the PCR technique necessitates costly and specialized equipment to facilitate the thermal-cycling amplification process, as well as skilled personnel to ensure accurate detection.[6] These limitations of the PCR technique restrict its application in resource-limited settings. Therefore, there is a pressing need to explore more accessible and cost-effective methods for nucleic acid assays.

DNA nanomachines are synthetic molecular devices that draw inspiration from the natural molecular motors found within living organisms.[7] These nanomachines are composed of assembled DNA structures that execute mechanical movements at the micro- or nanoscale. The utilization of DNA oligonucleotides as the fundamental building blocks of DNA nanomachines confers several distinct advantages. These oligonucleotides can be chemically synthesized, thermally renatured, and easily modified, facilitating the construction and characterization of DNA nanomachines.[8] Furthermore, the inherent predictability and programmability of DNA oligonucleotides allow for the assembly of various DNA nanostructures based on specific base pairing, enabling the incorporation of designer functionalities.[9] As a result of these characteristics, a range of DNA nanomachines has been developed, each exhibiting diverse functionalities. Examples include DNA tweezers,[10] DNA walkers,[11] DNA motors,[12] and DNA robots,[13] which have been employed for applications such as target detection, molecular diagnosis, and in vivo imaging. DNA nanomachines hold significant promise for the advancement of sensor technologies and offer a versatile approach for the detection of gene fragments in nucleic acid assays.

[a] Institute of Biophysics, School of Pharmacy, Dezhou University, Dezhou 253023, China. Email: liwei_91@126.com, wangrui19920426@163.com
[b] College of Pharmaceutical Science, Hebei University, Baoding 071002, China
Supplementary Information available: [Material and reagents, gel electrophoresis analysis, optimization of experimental conditions, analytical performance for SARS-CoV-2 gene fragments, and generalizability]. See DOI: 10.1039/x0xx00000x

View Article Online DOI: 10.1039/D5AY01118C

Among the diverse array of DNA nanomachines, DNA tweezers are distinguished by their unique ability to exist in two distinct states, allowing them to open and close in a precise and predictable manner in response to specific stimuli.[10,14] Consequently, DNA tweezers can function as switches that detect external stimuli and generate measurable signals. Specifically, in the absence of particular stimuli, the DNA tweezer remains in an open state, effectively rendering the switch in the "off" position, which results in no signal output. Conversely, when exposed to specific stimuli, the DNA tweezer transitions to a closed state, activating the switch and facilitating signal generation. Alternatively, the design can be inverted, wherein the DNA tweezer is closed in the "off" position, producing no signal, and opens in the "on" position, resulting in signal production. However, a limitation of DNA tweezers is their inability to amplify signals; thus, when utilized as switches, the ratio of target to signal is typically 1:1, which often leads to low detection sensitivity and constrains their practical applications. Isothermal amplification techniques are widely employed in biosensing due to their ease of operation and significant amplification capabilities.[10b,15] These amplification processes occur at a constant temperature, allowing for the direct amplification of target gene fragments, particularly RNA entities, without the need for reverse transcription. Therefore, isothermal amplification presents a viable method for enhancing the signal between the target and the DNA switch.

This study presents an innovative isothermal amplification-bridged ratiometric DNA switch designed for the detection of viral gene fragments. The DNA switch is constructed from three specifically engineered single-stranded oligonucleotides, functioning analogously to a DNA tweezer: a central strand that is dual-labeled with donor and acceptor fluorophores, and two arm strands that possess overhangs complementary to the products of isothermal amplification. The detection process is delineated into two distinct phases. The initial phase involves binding-induced isothermal amplification, which is initiated by the target gene fragment; during this phase, the target gene fragment is converted into amplification products at a predetermined ratio of 1:1250. The subsequent phase is the signal generation phase, which is triggered by the amplification products. In this phase, the DNA switch is activated, resulting in the transition of the open DNA tweezer to a closed state, thereby enhancing the FRET efficiency between the donor and acceptor fluorophores and producing a ratiometric fluorescent signal. Due to the effective conversion of the target facilitated by isothermal amplification, one target gene fragment is transformed into approximately 1250 DNA products, which can subsequently bind to 1250 DNA switches, leading to the generation of amplified ratiometric fluorescent signals. Consequently, this method enables the sensitive detection of the SARS-CoV-2 gene fragment (ORF1ab) with a detection limit of 0.05 fM. Analysis of actual samples from patients exhibiting upper respiratory symptoms indicates the method's potential for clinical diagnostic applications. Furthermore, by modifying the recognition strands, the method also allows for the sensitive and selective detection of the RABV gene fragment, demonstrating its versatility and adaptability. Thus, this research offers a novel and sensitive approach for the detection of viral gene fragments, holding significant promise for the clinical diagnosis of infectious diseases.

2. Experimental

2.1 Preparation of the DNA switch

The DNA oligonucleotides were reconstituted in TE buffer, comprising 10 mM Tris and 1 mM Na_2EDTA, adjusted to a pH of 8.0, resulting in a concentration of 50 μM. Subsequently, 6 μL of H-DNA (50 μM), 6 μL of A-DNA (50 μM), and 6 μL of B-DNA (50 μM) were subjected to annealing in 182 μL of TAE/Mg buffer, which contains 40 mM Tris, 20 mM acetic acid, 2 mM EDTA, and 12.5 mM magnesium acetate, also at a pH of 8.0. This process involved heating the mixture to 90 °C for 10 min, followed by a gradual cooling to 30 °C. The resulting initial DNA switch was established in the "off" state, achieving a final concentration of 1.5 μM.

2.2 Detection of viral gene fragments

The isothermal amplification induced by binding was initially conducted using a 1× Klenow buffer. The reaction system, totaling 30 μL, comprised 2 μL of target viral gene fragments at various concentrations, 2 μL of R1, 2 μL of R2, 1 μL of dNTPs at a concentration of 2.5 mM, 2 μL of Klenow Fragment (KF) at 1 U/μL, 5 μL of Nt.BbvCI at 1 U/μL, 3 μL of 10× Klenow buffer, and 13 μL of DEPC-treated water. Notably, the concentration ratios were maintained at 1:2 for the target to R1 and 1:2.5 for the target to R2. The mixture was incubated at 37 °C for 60 min, followed by a heat inactivation step at 80 °C for 10 min to terminate the reaction. Subsequently, 10 μL of a DNA switch at a concentration of 1.5 μM was introduced into the mixture and incubated at 37 °C for an additional 50 min. Fluorescence spectra were then recorded over a wavelength range of 505 nm to 650 nm using a fluorescence spectrophotometer (F-7000, Hitachi, Japan). The excitation wavelength was established at 485 nm, with the photomultiplier tube (PMT) voltage set to 400 V and the bandwidth fixed at 10 nm. The fluorescence intensities of the donor fluorophore (FI_D) and the acceptor fluorophore (FI_A) were measured at 518 nm and 586 nm, respectively, and the ratio of FIA to FID (FI_A/FI_D) in both the positive and negative systems was utilized for quantification purposes.

2.3 Actual sample assay

Initially, throat swabs were employed to obtain viral samples from patients presenting with upper respiratory tract symptoms. Subsequently, viral gene fragments were isolated utilizing the TIANamp Virus RNA Kit, in accordance with the manufacturer's instructions. Following this extraction process, 2 μL of the isolated gene fragments was analysed in accordance with the established detection protocol.

3. Results and discussion

3.1 Operational principle

View Article Online
DOI: 10.1039/D5AY01118C

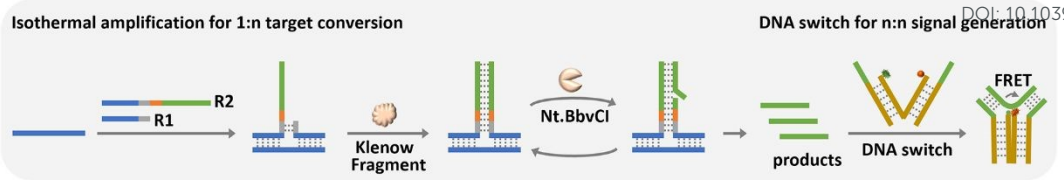

Scheme 1. Schematic illustration of the isothermal amplification-bridged DNA switch for the detection of viral gene fragments.

The operational mechanism of the isothermal amplification-bridged DNA switch for the detection of viral gene fragments is depicted in Scheme 1. The detection process is divided into two distinct phases: (1) binding-induced isothermal amplification and (2) activation of the DNA switch. In the initial phase, an isothermal amplification strategy is implemented to facilitate the sensitive detection of low-abundance viral gene fragments during the early stages of infection. Two recognition sequences, designated R1 and R2, are specifically designed to target gene fragment. Each sequence comprises 12 bases that are complementary to the target (indicated in blue) and 8 bases that are complementary to one another (indicated in grey). In the absence of the target, R1 and R2 are unable to hybridize due to the low binding affinity conferred by the 8 complementary bases. Conversely, when the target is present, the simultaneous recognition of the target by R1 and R2 promotes their proximity hybridization. Subsequently, with the assistance of the DNA polymerase KF, primer extension reactions occur, wherein R1 functions as the primer and R2 serves as the template, resulting in the generation of double-stranded DNA products. Notably, the extended portion of R1 is engineered to include a nicking site, which facilitates subsequent cleavage by the endonuclease Nt.BbvCI. The KF then continues to drive the extension reaction at the nicking site, replacing the cleaved products and leading to further nicking by Nt.BbvCI. Consequently, through a series of extension-nicking cycles, a substantial quantity of single-stranded DNA products is produced. This phase culminates in a target conversion, wherein a single target gene fragment is transformed into numerous ssDNA products.

In the second phase, the DNA switches are designed with a central strand known as H-DNA, accompanied by two arm strands, A-DNA and B-DNA. This configuration includes a 2-base hinge that serves as a flexible region for conformational changes, as well as two single-stranded overhangs (indicated in green) that function as recognition sequences for the DNA products. Additionally, a fluorescence donor (FAM, represented by a green spark) and an acceptor (TAMRA, depicted as an orange dot) are concurrently labeled on the H-DNA. Initially, the DNA switch exists in an "off" state, wherein the fluorescence donor and acceptor are spatially separated, resulting in low FRET efficiency, which typically occurs between two fluorophores through dipole-dipole interactions.[16] However, upon interaction with the DNA products, these products hybridize with the two arm overhangs in a cooperative manner, inducing a conformational change in the DNA switch to an "on" state. This transition brings the fluorescence donor and acceptor closer together, thereby enhancing FRET efficiency.

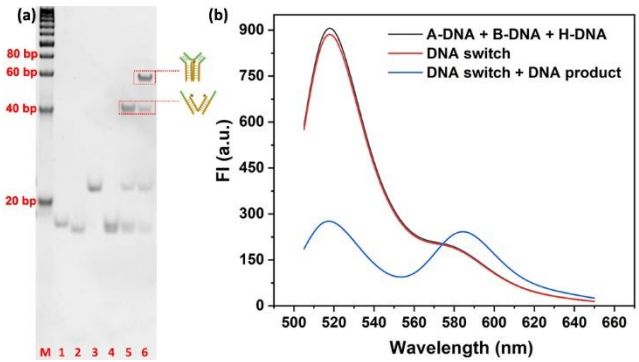

Fig. 1 (a) Gel electrophoresis diagram illustrating the assembly of the DNA switch. Lane 1: A-DNA; lane 2: B-DNA; lane 3: H-DNA; lane 4: A-DNA + B-DNA; land 5: A-DNA + B-DNA + H-DNA; lane 6: A-DNA + B-DNA + H-DNA + DNA product; lane M: 20 bp DNA ladder marker. (b) Fluorescence spectra of the DNA switch under different conditions.

This phase concludes with the generation of signals, during which multiple DNA products activate various DNA switches, resulting in the production of numerous ratiometric fluorescence signals. The fluorescence intensity ratio (FI_A/FI_D) is calculated by dividing the acceptor emission intensity by the donor emission intensity, which is directly correlated to the quantity of the target gene fragment present.

3.2 Characterization of the DNA switch

The DNA switch was engineered to exhibit an "off" state in the absence of DNA products and an "on" state in their presence, which was indicated by a change in fluorescence signal. The initial assembly of the DNA switch and its subsequent transformation were validated using native polyacrylamide gel electrophoresis (Native-PAGE) and fluorescence spectroscopy. As illustrated in Fig. 1a, distinct electrophoretic bands were identified in lanes 1, 2, 3, and 4, corresponding to A-DNA, B-DNA, H-DNA, and the combination of A-DNA and B-DNA, respectively. Lane 5 presents a mixture of A-DNA, B-DNA, and H-DNA subjected to an annealing process, where a novel band with a slower migration rate is observed, indicating the formation of the initial DNA switch. Fig. 1b demonstrates that the fluorescence spectra of the assembled DNA switch show minimal variation compared to the mixture of A-DNA, B-DNA, and H-DNA, thereby confirming that the initially assembled DNA switch is in an "off" state characterized by low FRET. Upon the introduction of the DNA product, a new band

View Article Online
DOI: 10.1039/D5AY01118C

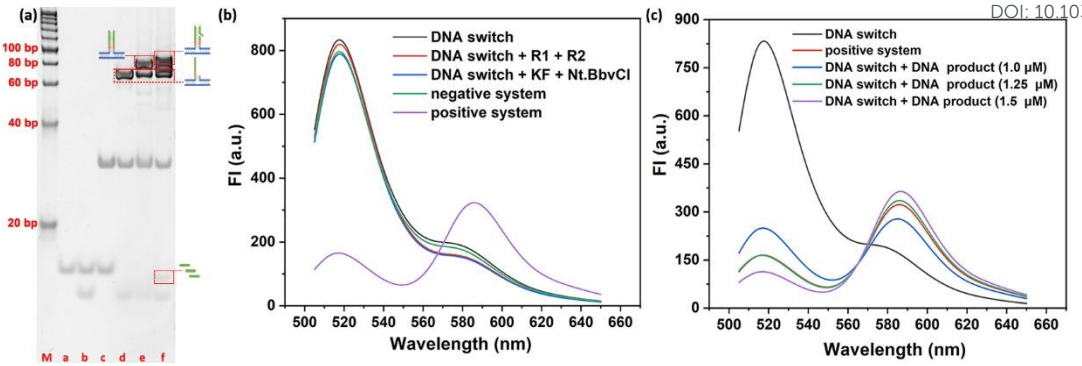

Fig. 2 (a) Gel electrophoresis diagram illustrating the process of binding-induced isothermal amplification. Lane a: ORF1ab gene fragment; lane b: ORF1ab gene fragment + R1; lane c: ORF1ab gene fragment + R2; lane d: ORF1ab gene fragment + R1 + R2; lane e: ORF1ab gene fragment + R1 + R2 + KF + dNTPs; lane f: ORF1ab gene fragment + R1 + R2 + KF + dNTPs + Nt.BbvCI; lane M: 20 bp DNA ladder marker. (b) Fluorescence spectra of the detection system under different conditions. (c) Fluorescence spectra of the positive control system and the DNA switches with varying amounts of DNA products.

exhibiting the slowest migration rate is observed in Fig. 1a, signifying the interaction between the DNA switch and the DNA product. The corresponding fluorescence spectra in Fig. 1b reveal a significant increase in FRET, further indicating the conformational transition of the DNA switch to the "on" state, characterized by high FRET. These findings substantiate the successful assembly of the conceptual DNA switch and its ability to transition from the "off" state to the "on" state upon activation by DNA products.

3.3 Feasibility verification

The ORF1ab gene fragment, a conserved sequence within the SARS-CoV-2, serves as the analytical model in this study. The isothermal amplification induced by target binding was initially characterized using native polyacrylamide gel electrophoresis (PAGE). As illustrated in Fig. 2a, lane a displays the ORF1ab gene fragment, lane b shows the combination of the ORF1ab gene fragment and R1, while lane c depicts the mixture of the ORF1ab gene fragment and R2, with distinct electrophoretic bands observed for each component. Lane d presents the mixture of the ORF1ab gene fragment, R1, and R2, revealing a novel electrophoretic band. These findings confirm that target recognition is facilitated by R1 and R2, allowing for the formation of a three-way junction structure. The introduction of KF and dNTPs in lane e results in the emergence of a novel electrophoretic band exhibiting a slower migration rate, indicative of the extension reaction's activity. Furthermore, the addition of Et.BbvCI in lane f yields a set of electrophoretic bands with the slowest migration, suggesting that the DNA products are being replaced as a result of the extension reactions. Additionally, a novel electrophoretic band with a relatively rapid migration rate is also observed, further supporting the release and production of DNA products. These results validate the feasibility of the proposed binding-induced isothermal amplification strategy. Moreover, fluorescence spectra were recorded under various conditions to assess the viability of the proposed method for detecting the ORF1ab gene fragment. As demonstrated in Fig. 2b, the control system containing only the DNA switch and the negative system, which included all components except the target, exhibited minimal FRET. Furthermore, to evaluate the potential interference, the mixture comprising the DNA switch, R1, and R2, in conjunction with the mixture containing the DNA switch, KF, and Nt.BbvCI, was also analyzed. The fluorescence responses exhibited minimal variation, indicating that the stable background is primarily attributed to the DNA switch. In contrast, the positive system displayed significant FRET, indicating the effectiveness of the proposed method for the detection of the target gene fragment.

3.4 Analysis of target conversion efficiency

The isothermal amplification process is designed to enhance detection sensitivity by converting a single target gene fragment into multiple DNA products. Given that the efficiency of target conversion directly influences sensitivity, an analysis was conducted utilizing DNA switches alongside specific quantities of DNA products. As illustrated in Fig. 2c, the fluorescence spectra of the mixture containing DNA switches and DNA products at a concentration of 1.25 μM closely aligns with that of the positive control system containing 1.0 nM of the ORF1ab gene fragment. Consequently, it can be inferred that the 1.0 nM ORF1ab gene fragment in the detection system was successfully transformed into 1.25 μM of DNA products via the implemented isothermal amplification process, resulting in a target conversion efficiency of 1:1250.

3.5 Optimization of experimental conditions

In order to optimize analytical performance, a systematic evaluation of various experimental parameters was conducted. These parameters included the ratios of the target gene fragment to R1 and R2, the dosages of KF and Nt.BbvCI, the concentration of the DNA switch, and the reaction times for isothermal amplification and DNA switch. The initial assessment revealed that the quantities of R1 and R2 significantly influence target binding, which subsequently impacts the isothermal

View Article Online
DOI: 10.1039/D5AY01118C

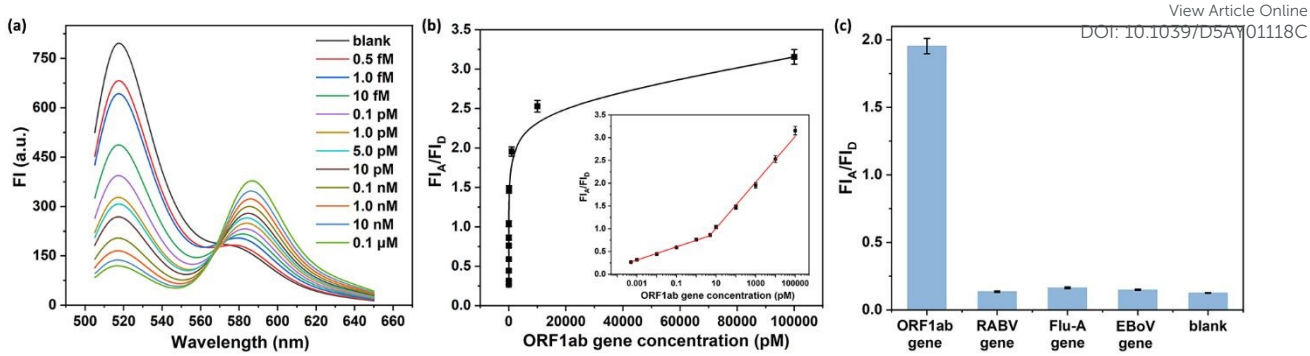

Fig. 3 (a) Fluorescence spectra of the detection system at varying concentrations of the ORF1ab gene fragment. (b) FI_A/FI_D responses of the detection system at different concentrations of the ORF1ab gene fragment. The inset illustrates the linear relationship between the FI_A/FI_D response and the concentration of the ORF1ab gene fragment. (c) FI_A/FI_D responses generated by various viral gene fragments. The error bar indicates the standard deviation derived from three parallel measurements.

amplification process. Consequently, the ratios of the ORF1ab gene fragment to R1 and R2 were analyzed. As illustrated in Figs. S1 and S2, the FI_A/FI_D exhibited a gradual increase, plateauing as the ratios of R1 and R2 were elevated. Therefore, a ratio of 1:2 was determined to be optimal for R1, while a ratio of 1:2.5 was deemed optimal for R2. The dosages of KF and Nt.BbvCI were found to primarily influence the extension and nicking reactions during amplification; thus, these dosages were also evaluated. Fig. S3 demonstrates that the FI_A/FI_D increased progressively with the enhancement of KF, reaching a plateau at a dosage of 2.0 U, which was selected as the optimal dosage. Similarly, Fig. S4 indicates that the FI_A/FI_D increased with the dosage of Nt.BbvCI, achieving a plateau at 5.0 U, which was chosen as the optimal dosage for this enzyme.

The DNA switch plays a pivotal role in signal generation, necessitating an adequate concentration for the effective detection of DNA products resulting from amplification. The optimization of DNA switch concentration revealed, as shown in Fig. S5, that the FI_A/FI_D increased and plateaued at a concentration of 1.5 μM, which was selected as optimal. Furthermore, reaction times are critical for ensuring the completeness of reactions; thus, the reaction durations for isothermal amplification and DNA switch were assessed. Figs. S6 and S7 indicate that the FI_A/FI_D reached its maximum at a reaction time of 60 min for isothermal amplification and 50 min for the DNA switch. Consequently, these durations were selected for subsequent experimental procedures.

3.6 Analytical performance for SARS-CoV-2 gene fragment

Under optimal experimental conditions, the analytical performance of the proposed method for detecting SARS-CoV-2 gene fragments was evaluated. The initial assessment focused on sensitivity, specifically through the detection of the ORF1ab gene fragment at varying concentrations. As illustrated in Fig. 3a, fluorescence spectra were recorded for the detection system across a concentration range of 0.5 fM to 0.1 μM. The results indicated a gradual decrease in fluorescence intensity of the FAM donor, accompanied by a corresponding increase in the TAMRA acceptor, thereby demonstrating a positive correlation between target concentration and the efficacy of the isothermal amplification-bridged DNA switch. Within this concentration range, two distinct linear relationships were established between the FI_A/FI_D and the logarithm of the concentrations, as demonstrated in Fig. 3b. The first relationship, applicable from 0.5 fM to 5.0 pM, yielded a linear correlation equation of FI_A/FI_D = 0.75 + 0.14 lgC, with a coefficient of determination (R^2) of 0.997. The second relationship, valid from 5.0 pM to 0.1 μM, produced a correlation equation of FI_A/FI_D = 0.51 + 0.50 lgC, with an R^2 of 0.996. It is hypothesized that the existence of these two linear relationships may be attributed to differing capacities for triggering isothermal amplification at high versus low target concentrations. Notably, both linear relationships converge at 5.0 pM, suggesting that for concentrations below 0.5 pM, the lower concentration linear relationship may be utilized, while for concentrations exceeding 5.0 pM, the higher concentration linear relationship is applicable. Employing the triple standard deviation (3σ) criterion, a limit of detection of 0.04 fM was determined. This sensitivity for viral gene fragment detection is comparable to, or exceeds, that of previously reported methodologies, as detailed in Table S2. A distinctive feature of the proposed method is its extensive linear range, spanning approximately eight orders of magnitude and encompassing two linear relationships. This characteristic renders the method particularly suitable for the detection of viral gene fragments across various biological samples, where target gene fragment levels may vary significantly.

To further assess the specificity of the proposed methodology, fluorescence responses were measured for the ORF1ab gene fragment at a concentration of 1.0 nM, in conjunction with various interfering gene fragments, including those from the RABV, influenza A virus (Flu-A), and Ebola virus (EBoV), all at a concentration of 10 nM. As illustrated in Fig. 3c, only the target ORF1ab gene fragment elicited a significant FRET response, while the interfering gene fragments produced FRET responses that were comparable to those of the blank control. Moreover, a t-test was conducted to compare the target group with the interference groups, indicating a statistically significant difference between the target group and the interference group ($p \leq 0.05$). These findings indicate that the proposed method

View Article Online
DOI: 10.1039/D5AY01118C

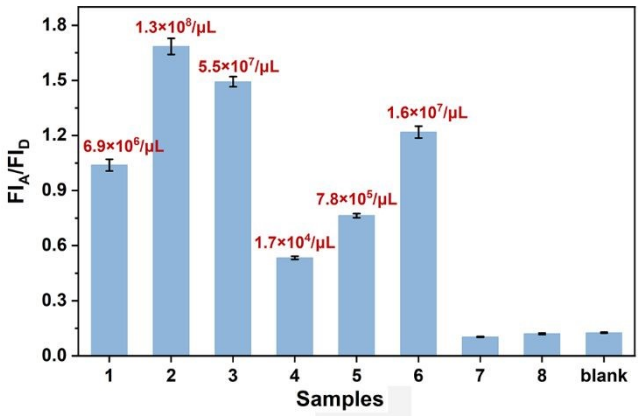

Fig. 4 FI_A/FI_D responses and the detected quantity of the ORF1ab gene fragment in actual samples from patients exhibiting upper respiratory symptoms. The error bar indicates the standard deviation derived from three parallel measurements.

demonstrates a high degree of specificity for the detection of the ORF1ab gene fragment.

To evaluate the precision of this method for detecting the ORF1ab gene fragment, both intra-assay and inter-assay analyses were performed using three samples containing 10 fM, 5.0 pM, and 1.0 nM of the ORF1ab gene fragment. The relative standard deviations (RSDs) for the intra-assay were found to be 2.7%, 1.8%, and 4.3%, while the RSDs for the inter-assay were 3.4%, 3.7%, and 4.7%, respectively, as detailed in Tables S3 and S4. These results suggest that the designed method exhibits acceptable levels of repeatability and reproducibility for the detection of the ORF1ab gene fragment. Additionally, to assess the accuracy of this methodology, a recovery experiment was performed utilizing three human serum samples that contained concentrations of the ORF1ab gene fragment at 10 fM, 5.0 pM, and 1.0 nM, respectively. The findings, detailed in Table S5, demonstrated recoveries of 95.7%, 98.8%, and 93.5%, accompanied by RSDs of 3.2%, 3.0%, and 4.2%, respectively. These results indicate that the proposed method exhibits an acceptable level of accuracy for the detection of viral gene fragments, suggesting its potential applicability in clinical settings.

3.7 Actual sample assay

To assess the practical applicability of the proposed methodology, throat swab samples were collected from patients exhibiting upper respiratory tract symptoms as well as from healthy volunteers. Viral RNA was extracted from these samples utilizing a virus RNA extraction kit. The fluorescence responses of the samples were recorded in accordance with the proposed method, and the concentrations of the detected ORF1ab gene fragment were subsequently quantified using established regression equations. A total of 25 throat swab samples were collected from patients with upper respiratory tract symptoms. As depicted in Fig. 4, six of the samples (samples 1-6) tested positive for the ORF1ab gene, with the detected quantities of ORF1ab gene fragments ranging from 1.7 × 10^4 to 1.3 × 10^8 copies/μL. In contrast, samples 7 and 8, obtained from healthy donors, yielded negative results, which were consistent with the blank control. Additionally, t-test was also conducted to compare the positive group with the negative group. The results indicated a statistically significant difference between the positive and negative groups ($p \leq 0.05$). Therefore, the proposed methodology exhibits a high degree of reliability for the detection of actual samples and shows significant promise for utilization in the clinical diagnosis of viral infections.

3.8 Generalizability

To evaluate the generalizability of the proposed methodology, the detection of a gene fragment from the RABV was conducted by modifying the recognition sequences. RABV is known to cause fatal encephalitis, and currently, there are no effective treatment options available.[17] Therefore, the early detection of RABV is crucial for enabling timely control measures and ensuring public health safety.[10b,18] The detection of RABV gene fragments serves as an effective approach for identifying RABV infections. Consequently, the detection of RABV gene fragments was chosen as the model for assessing the generalizability of the proposed method. As illustrated in Fig. S8, the initiation of the isothermal amplification process by the RABV gene fragment was characterized using native-PAGE, which confirmed that the RABV gene fragment successfully induced the formation of a three-way junction structure, leading to subsequent extension and cleavage reactions, as well as the production of single-stranded DNA products necessary for the activation of DNA switches. Furthermore, to further explore the applicability of the proposed method for RABV gene fragment detection, fluorescence spectra were recorded under various conditions. As shown in Fig. S9, the control system, which contained only the DNA switch, and the negative system, which included all components except the target RABV gene fragment, exhibited minimal FRET. In contrast, the positive system demonstrated significant FRET, thereby indicating the feasibility of the proposed method for detecting the RABV gene fragment by modulating the recognition sequences.

The sensitivity of the proposed methodology for the detection of the RABV gene fragment was assessed by analyzing its performance across a range of concentrations. As depicted in Fig. 5a, fluorescence spectra were recorded from concentrations spanning 0.5 fM to 0.1 μM, revealing a progressive decline in the fluorescence intensity of the FAM donor, accompanied by a corresponding increase in the fluorescence intensity of the TAMRA acceptor. This observation underscores the positive correlation between target concentration and the effectiveness of the isothermal amplification-bridged DNA switch. Within the specified concentration range, two distinct linear relationships were established between the FI_A/FI_D and the logarithm of the concentrations, as illustrated in Fig. 5b. The first relationship, applicable from 0.5 fM to 5.0 pM, yielded a linear correlation equation of FI_A/FI_D = 0.78 + 0.16 lgC, with a coefficient of determination (R^2) of 0.994. The second relationship, valid from 5.0 pM to 0.1 μM, produced a correlation equation of FI_A/FI_D = 0.59 + 0.46 lgC, with an R^2 of 0.995. Utilizing the 3σ criterion, the limit of detection for RABV was established at 0.08 fM. The

View Article Online
DOI: 10.1039/D5AY01118C

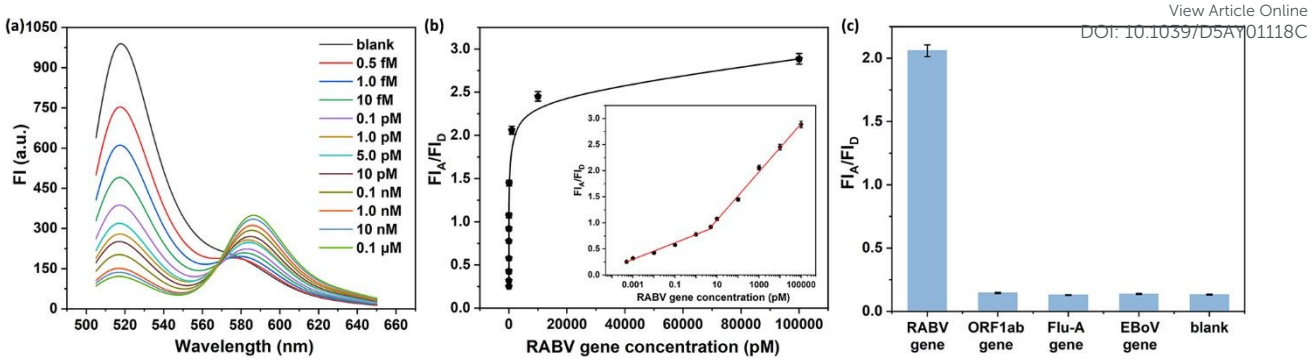

Fig. 5 (a) Fluorescence spectra of the detection system at varying concentrations of RABV gene fragments. (b) FI_A/FI_D responses of the detection system with different concentrations of RABV gene fragments. The inset illustrates the linear relationship between the FI_A/FI_D response and the concentration of RABV gene fragments. (c) FI_A/FI_D responses generated by various viral gene fragments. The error bar indicates the standard deviation derived from three parallel measurements.

characteristics of the linear range, linear relationships, and detection limit for the RABV gene fragment are consistent with those observed for the ORF1ab gene fragment, thereby reinforcing the feasibility and reliability of the proposed method for the detection of various viral gene fragments. Furthermore, to evaluate the specificity of the proposed method for RABV gene fragment detection, fluorescence responses were measured for the RABV gene fragment, alongside various interfering gene fragments. As shown in Fig. 5c, only the target RABV gene fragment produced a significant FRET response, while the interfering gene fragments exhibited FRET responses comparable to those of the blank control. A t-test was also conducted, indicating a statistically significant difference between the target group and the interference groups ($p \leq 0.05$). The findings suggest that the design targeting the RABV gene fragment exhibits a significant level of specificity in the detection of the RABV gene fragment.

The precision of the proposed method for the detection of RABV gene fragments was evaluated through both intra-assay and inter-assay analyses, utilizing three samples with concentrations of 10 fM, 5.0 pM, and 1.0 nM of the RABV gene fragment. The RSDs for both intra-assay and inter-assay measurements were consistently below 5.0%, as presented in Tables S6 and S7, indicating satisfactory levels of repeatability and reproducibility in the detection of the RABV gene fragment. Additionally, to further assess the accuracy of this methodology, a recovery experiment was conducted using three human serum samples containing the RABV gene fragment at concentrations of 10 fM, 5.0 pM, and 1.0 nM, respectively. The results, summarized in Table S8, revealed recoveries of 101.3%, 96.4%, and 98.1%, with corresponding RSDs of 2.9%, 3.4%, and 3.8%. These findings suggest that the proposed method demonstrates an acceptable level of accuracy for the detection of RABV gene fragments.

Conclusions

In conclusion, this study presents the development of an isothermal amplification-bridged DNA switch designed for the detection of viral gene fragments. To address the limitations associated with the 1:1 signal output mode of conventional DNA switches, an isothermal amplification strategy was implemented to convert the target into multiple DNA products. The conversion efficiency was quantified at 1:1250, demonstrating a substantial signal amplification capability that facilitates the sensitive detection of the SARS-CoV-2 gene fragment ORF1ab, with a limit of detection of 0.04 fM. The method exhibited an extensive linear range spanning approximately eight orders of magnitude, characterized by two distinct linear relationships, thereby making it particularly effective for detecting viral gene fragments in diverse biological samples where target gene fragment concentrations may vary considerably. Furthermore, quantitative analysis of the ORF1ab gene fragment was conducted using actual samples from patients exhibiting upper respiratory symptoms, highlighting the method's significant clinical applicability in the diagnosis of infectious diseases. Additionally, by modifying the recognition sequences, the method achieved sensitive and selective detection of viral gene fragments from RABV, with a limit of detection of 0.08 fM, indicating the broad applicability of the proposed DNA switch. Consequently, this approach offers a novel and highly sensitive methodology for the detection of viral gene fragments, holding considerable promise for clinical diagnosis and screening of viral infections.

Author contributions

Wei Li: Conceptualization, Methodology, Funding acquisition, Writing-Original Draft; Jiayue Li: Investigation, Validation, Date curation; Shang Sun: Resource, Funding acquisition; Manman Duan: Formal analysis, Funding acquisition; Meng Wang: Software; Rui Wang: Funding acquisition, Writing – review & editing, Project administration.

Conflicts of interest

There are no conflicts to declare.

Data availability

Data will be made available on request.

Ethical statement

Informed consent was obtained from all human participants involved in the study.

Acknowledgements

This work was supported by the National Natural Science Foundation of China (82403694 and 62301110), the Natural Science Foundation of Shandong Province (ZR2024QH631), the Qingchuang Science and Technology Plan of Shandong Province (2024KJG072) and the Talent Incubation Project of Dezhou University (2024xjrc118 and 2024xjrc160).

References

1 (a) T. Zhang, R. Deng, Y. Wang, C. Wu, K. Zhang, C. Wang, N. Gong, R. Ledesma-Amaro, X. Teng, C. Yang, T. Xue, Y. Zhang, Y. Hu, Q. He, W. Li and J. Li, Nat. Biomed. Eng., 2022, 6, 957–967; (b) X. Zhang, G. Li, G. Chen, N. Zhu, D. Wu, Y. Wu and T.D. James, Med. Res. Rev., 2021, 41, 2039–2108; (c) Y. Zhang, J. Chen, F. Kong, C. Wang, H. Guo, Y. Li, J. Lu, J. Zhang, J. Wang and Y. Zhou, Langmuir, 2024, 40, 11534–11540.

2 S. Gong, S. Zhang, X. Wang, J. Li, W. Pan, N. Li and B. Tang, Anal. Chem., 2021, 93, 15216–15223.

3 (a) K. Liu, D. Pan, Y. Wen, H. Zhang, J. Chao, L. Wang, S. Song, C. Fan and Y. Shi, Small, 2018, 14, 1701718; (b) V. Krivitsky, M. Zverzhinetsky and F. Patolsky, Nano Lett., 2016, 16, 6272–6281.

4 P. Moitra, M. Alafeef, K. Dighe, M.B. Frieman and D. Pan, ACS Nano, 2020, 14, 7617–7627.

5 (a) M.M. Kaminski, O.O. Abudayyeh, J.S. Gootenberg, F. Zhang and J.J. Collins, Nat. Biomed. Eng., 2021, 5, 643–656; (b) D. Dutta, S. Naiyer, S. Mansuri, N. Soni, V. Singh, K.H. Bhat, N. Signh, G. Arora and M.S. Mansuri, Diagnostics, 2022, 12, 1503.

6 J. Song, L. Zhang, L. Zeng and X. Xu, Anal. Chem., 2023, 95, 11187–11192.

7 (a) M. Xiao, K. Zou, L. Li, L. Wang, Y. Tian, C. Fan and H. Pei, Angew. Chem., 2019, 131, 15594–15600; (b) C. Jung, P.B. Allen and A.D. Ellington, Nat. Nanotechnol., 2016, 11, 157–163; (c) J.X. Dong, S.M. Zhang, Y.L. Li, X. Zhang, Y.J. Fan, M. Su, Z.G. Wang, H. Li, S.G. Shen, Z.F. Gao, Q. Wei and F. Xia, Anal. Chem., 2023, 95, 16744–16753.

8 (a) A. Yildiz, M. Tomishige, R.D. Vale and P.R. Selvin, Science, 2004, 303, 676–678; (b) P. Zhan, A. Peil, Q. Jiang, D. Wang, S. Mousavi, Q. Xiong, Q. Shen, Y. Shang, B. Ding, C. Lin, Y. Ke and N. Liu, Chem. Rev., 2023, 123, 3976–4050; (c) S. Yang, L. Zhou, Z. Fang, Y. Wang, G. Zhou, X. Jin, Y. Cao and J. Zhao, ACS Sens., 2024, 9, 2194–2202.

9 (a) P. Shen, Y. Ji, X. Yue, Y. Li, M. Han, Y. Ma, M. Meng, F. Fan and S. Chang, Sens. Actuat. B: Chem., 2025, 428, 137252; (b) D. Fu, R.P. Narayanan, A. Prasad, F. Zhang, D. Williams, J.S. Schreck, H. Yan and J. Reif, Sci. Adv., 2022, 8, eade4455; (c) M. Liu, Q. Zhang, Z. Li, J. Gu, J.D. Brennan and Y. Li, Nat. Commun., 2016, 7, 12074.

10 (a) N. Zhang, H. Cheng and Y. Liu, Anal. Chem., 2024, 96, 15355–15363; (b) S. Liu, C. Wang, Z. Wang, K. Xiang, Y. Zhang, G.C. Fan, L. Zhao, H. Han and W. Wang, Biosens. Bioelectron., 2022, 204, 114078; (c) W. Li, Y. Bai, M. Wang, R. Wang, Y. Wu and Z. Wang, Microchem. J., 2024, 204, 111157.

11 (a) H. Jiang, S. Qi, B. Ang, I.M. Khan, X. Dong, Z. Wang and J. Yang, Chem. Eng. J., 2025, 514, 163177; (b) Z. Sun, L. Han, Y. Yin, Y. Mou, Y. Tian, W. Zhang, D. Chen, Y. Wu, X. Sun, Y. Guo and F. Li, Biosens. Bioelectron., 2025, 280, 117446.

12 (a) W. Li, S. Wang, M. Lin, X. Chen, J. Li, W. Cui and R. Wang, Biosens. Bioelectron., 2025, 273, 117186; (b) X. Zhong, J. Hua, M. Shi, Y. He, Y. Huang, B. Wang, L. Zhang, S. Zhao, L. Hou and H. Liang, ACS Sens., 2024, 9, 1280–1289.

13 H. Li, J. Gao, L. Cao, X. Xie, J. Fan, H. Wang, H.H. Wang and Z. Nie, Angew. Chem. Int. Ed., 2021, 60, 26087–26095.

14 (a) B. Yurke, A.J. Turberfield, A.P. Mills, F.C. Simmel and J.L. Neumann, Nature, 2000, 406, 605–608; (b) M. Liu, J. Fu, C. Hejesen, Y. Yang, N.W. Woodbury, K. Gothelf, Y. Liu and H. Yan, Nat. Commun., 2013, 4, 2127.

15 (a) L. Zhang, T. Feng, Q. Liu, C. Zuo, Y. Wu, H. Zhao, H. Yu, D. Bai, X. Han, N. Yin, J. Pu, Y. Yang, J. Li, J. Guo, S. Deng and G. Xie, Biosens. Bioelectron., 2025, 273, 117183; (b) X. Zhang, H. Zhou, W. Hu, J. Zhang, J. Xu, X. Liu and J. Yan, Microchem. J., 2025, 213, 113834.

16 (a) V.V. Didenko, BioTechniques, 2001, 31, 1106–1121; (b) X. Xu, L. Wang, K. Li, Q. Huang and W. Jiang, Anal. Chem., 2018, 90, 3521–3530.

17 C.R. Fisher, D.G. Streicker and M.J. Schnell, Nat. Rev. Microbiol., 2018, 16, 241–255.

18 S.R. Silva, I.S.S. Katz, E. Mori, P. Carnieli, L.F.P. Vieira, H.B.C.R. Batista, L.B. Chaves and K.C. Scheffer, Biologicals, 2013, 41, 217–223.

View Article Online
DOI: 10.1039/D5AY01118C

Data availability

Data will be made available on request.